Experimental Studies of Droplet Evaporation Kinetics: Validation of Models for Binary and Ternary Aqueous Solutions

HUIWEN XUE

NOAA/Environmental Technology Laboratory, Boulder, Colorado

ALFRED M. MOYLE, NATHAN MAGEE, JERRY Y. HARRINGTON, AND DENNIS LAMB

Meteorology Department, The Pennsylvania State University, University Park, Pennsylvania

(Manuscript received 15 October 2004, in final form 24 May 2005)

ABSTRACT

Experiments were conducted with an electrodynamic levitation system to study the kinetics of droplet evaporation under chemically rich conditions. Single solution droplets of known composition (HNO_3/H_2O or $H_2SO_4/HNO_3/H_2O$) were introduced into an environmentally controlled cubic levitation cell. The gaseous environment was set intentionally out of equilibrium with the droplet properties, thus permitting the HNO_3 mass accommodation coefficient to be determined. Measurements were performed at room temperature and various pressures (200–1000 hPa). Droplet sizes (initial radii in the range 12–26 μm) were measured versus time to high precision (± 0.03 μm) via Mie scattering and compared with sizes computed by different models for mass and heat transfer in the transition regime. The best agreement between the theoretical calculations and experimental results was obtained for an HNO_3 mass accommodation coefficient of 0.11 ± 0.03 at atmospheric pressure, 0.17 ± 0.05 at 500 hPa, and 0.33 ± 0.08 at 200 hPa. The determination of the mass accommodation coefficient was not sensitive to the transport model used. The results show that droplet evaporation is strongly limited by HNO_3 and occurs in two stages, one characterized by rapid H_2O mass transfer and the other by HNO_3 mass transfer. The presence of a nonvolatile solute (SO_4^{2-}) affects the activities of the volatile components (HNO_3 and H_2O) and prevents complete evaporation of the solution droplets. These findings validate recent attempts to include the effects of soluble trace gases in cloud models, as long as suitable model parameters are used.

1. Introduction

The rates with which aqueous solution droplets grow and evaporate depend on the chemical and thermodynamic conditions prevailing at the time. The composition of the droplets affects their equilibrium vapor pressures, and the relative abundances of condensable gases influence how rapidly mass exchanges between the liquid and vapor phases. Numerical models of droplet condensation and evaporation rely on understanding the chemistry and physics of the processes involved, as well as on knowledge of the various parameters incorporated into the theory. Experimental studies, with their capability of measuring droplet evolution under clearly defined conditions, allow theories to be tested and parameters to be determined. Validated numerical calculations then serve to predict and elucidate important atmospheric phenomena.

Cloud formation involves complicated interactions between atmospheric motions, aerosol particles, and condensable vapors. The microphysical properties of clouds, such as droplet number concentration and size distribution, play important roles in the global radiation budget (Houghton et al. 2001), precipitation formation (Rosenfeld 2000), and cloud chemistry (Feingold and Kreidenweis 2002). The microphysical evolution of clouds has traditionally been thought to be determined by the atmospheric aerosol population and moisture abundance (Rogers and Yau 1989, p. 72), but trace gases can also affect cloud microstructure (Kulmala et al. 1997; Hegg 2000; Charlson et al. 2001; Xue and Feingold 2004).

Nitric acid, generated photochemically in the atmosphere (Seinfeld and Pandis 1998, p. 241), may be an

Corresponding author address: Dr. Huiwen Xue, NOAA/Environmental Technology Laboratory, 325 Broadway, Boulder, CO 80305.
E-mail: Huiwen.xue@noaa.gov

especially important trace gas (Charlson et al. 2001). The concentration of HNO_3 is expected to approach 1 ppbv in remote areas of the continents and exceed 50 ppbv in heavily polluted areas (Kulmala et al. 1993). Nitric acid, being highly soluble in water, acts to reduce the activity of water in the solution (Tang 1980; Clegg and Brimblecombe 1990). When traditional Köhler theory (Pruppacher and Klett 1997, p. 173) is modified to account for the presence of HNO_3, the critical supersaturation for a cloud condensation nucleus (CCN) to be activated and form a cloud droplet is found to be lowered substantially (Korhonen et al. 1996; Laaksonen et al. 1998; Charlson et al. 2001). Cloud models of the activation and growth of CCN in the lower troposphere have shown that the number of activated nuclei is increased and the mean size of cloud droplets is decreased by ambient concentrations of HNO_3 (Kulmala et al. 1993, 1995). Some studies have shown that modestly high gas-phase concentrations of HNO_3 can cause liquid aerosol particles to grow and yield persistent fogs, hazes, or clouds (Carslaw et al. 1994; Kulmala et al. 1997; Charlson et al. 2001). Thus, the albedo of the atmosphere may be increased by gas–droplet interactions (Nenes et al. 2002), although not in simple ways (Xue and Feingold 2004). Beyond effects on the radiation budget, HNO_3 may also affect precipitation microphysics. Hegg (2000) investigated precipitation formation in low-altitude clouds impacted by both HNO_3 and NH_3 and found precipitation to be enhanced, particularly by NH_3. Our current state of understandings of trace gas–cloud interactions is developing but still uncertain.

When HNO_3 is present at the time of cloud formation, vapors of both H_2O and HNO_3 are simultaneously transported to the surfaces of haze and cloud droplets. As these vapors are transferred into the liquid phase, the thermodynamical properties of the solutions are altered in complicated ways (Kim et al. 1993; Clegg et al. 1998). However, limited accommodation of the H_2O and HNO_3 molecules by the liquid surface can hinder the rate of mass transfer. The magnitude of the HNO_3 mass accommodation coefficient thus becomes an important parameter for quantitative studies of the effect of HNO_3 on atmospheric clouds. Lacking suitable data, some researchers have simply set such kinetic parameters to unity (e.g., Kulmala et al. 1993).

The binary cocondensation process has been studied in several ways. For instance, Rudolf et al. (2001) used a rapid-expansion chamber to study droplet growth on monodisperse di-2-ethyl-hexyl-sebacate (DEHS) aerosols in a supersaturated binary mixture of H_2O and HNO_3 vapors. The time-dependent sizes and number concentrations of the droplets were obtained optically (Wagner 1973). Comparing the experimentally determined droplet growth rates with model calculations and assuming the mass accommodation coefficient of H_2O to be unity, Rudolf et al. (2001) concluded that the mass accommodation coefficient of HNO_3 must be between 0.3 and 1.0.

This paper reports on new experimental investigations of binary cocondensation and evaporation using single, levitated droplets of binary (HNO_3/H_2O) and ternary ($H_2SO_4/HNO_3/H_2O$) solutions. We attempt to validate specific models of droplet growth and evaporation under representative conditions of temperature, total pressure, and partial vapor pressures. The present study does not attempt to invalidate the results of previous work. Rather, our goal is to determine the mass accommodation coefficient of HNO_3 under conditions that facilitate its direct application to atmospheric modeling. At the same time, we hope to provide experimental results that may lead to improved understanding of the mass accommodation process. Section 2 discusses the theory of mass and heat transfer to/from a droplet, while section 3 summarizes the experimental methods. The results are shown and discussed in section 4. Finally, section 5 concludes by emphasizing the need to define experimental conditions carefully when trying to establish values for the kinetic parameters used in cloud models.

2. Theoretical background

a. Aqueous phase equilibria

The equilibrium state of a droplet defines the conditions under which it neither grows by condensation nor evaporates. By the same reasoning, a droplet changes size only to the extent that the environmental conditions deviate from equilibrium. A robust designator of the equilibrium state is the set of activities of the various components comprising the solution. Thus, the activity A_i of a volatile component i is the effective mole fraction of i in the solution and is related to its equilibrium vapor pressure p_i^{eq} through a generalization of Raoult's Law, $A_i = p_i^{eq}/p_i^0$, where p_i^0 is the equilibrium vapor pressure of pure component i (Atkins 1986, p. 182). Note that activity is a property of the liquid phase, whereas the pressure ratio characterizes the conditions in the gas phase needed to maintain equilibrium. In the limiting case of pure water (never achieved in the atmosphere), $A_{H2O} = 1$, implying that $p_{H2O}^{eq} = p_{H2O}^0$, or in the convention of meteorology $e_{eq} = e_s$, which is the saturation vapor pressure of pure water.

All real solutions of atmospheric interest contain both volatile and nonvolatile solutes, so the activity of water in aqueous solutions is generally less than unity

(see Pruppacher and Klett 1997, p. 109). The activities of the solutes vary in complicated ways with their concentrations, chemical reactivity, and volatility (Stumm and Morgan 1981, section 2.9), and much literature has been devoted to quantifying the effects of aqueous phase chemical interactions on the activities of water and solutes of relevance to atmospheric systems (see Li and Coull 1948; Jaecker-Voirol et al. 1990; Kim et al. 1993; Zhang et al. 1993; Tabazadeh et al. 1994; Carslaw et al. 1995, 1997; Clegg et al. 1998). It is important that the equilibrium vapor pressures of all components be computed accurately, as the rates of droplet growth/evaporation are often proportional to small departures of the environmental partial pressures from the respective equilibrium values.

Factors other than composition also influence the equilibrium vapor pressures. The curvature of small droplets enhances the vapor pressure by the Kelvin equation (Pruppacher and Klett 1997, p. 170), and the pure-component vapor pressure (p_i^0) increases with temperature T by the Clausius–Clapeyron relationship (Pruppacher and Klett 1997, p. 117). Thus, given the function $p_i^0 = p_i^0(T)$, the equilibrium vapor pressure of i over a droplet of radius a becomes

$$p_{a,i} = p_i^0(T_a) A_i \exp\left(\frac{2\sigma_{l\upsilon}}{n_L R T_a a}\right), \tag{1}$$

where equilibrium at the droplet surface lets us set $p_i^{\text{eq}} = p_{a,i}$, $\sigma_{l\upsilon}$ is the surface tension, n_L is the molar density of the liquid, R is the universal gas constant, and T_a is the droplet temperature.

b. Interfacial exchange

Whenever the ambient conditions surrounding a droplet differ from the equilibrium state, the droplet will either accumulate mass and grow, or lose mass and evaporate. A net flux of molecules then crosses the liquid–vapor interface. A net flux of energy also exchanges between the two phases to compensate for the phase-change enthalpies. The molecular-scale mechanisms by which these exchanges of mass and energy occur are complicated and as yet highly uncertain (Davidovits et al. 1991, 1995; Li et al. 2001; Kolb et al. 2002), so surface processes are typically parameterized in terms of kinetic coefficients.

The mass accommodation coefficient and the thermal accommodation coefficient are the two conventional kinetic parameters used to account for the molecular interactions and energy exchanges at the liquid–gas interface. The mass accommodation coefficient, α_M, is defined as the probability that a vapor molecule impinging on the surface enters the liquid phase

$$\alpha_M = \frac{\text{flux of molecules entering the liquid phase}}{\text{flux of molecules colliding with the surface}}. \tag{2}$$

This ratio is sometimes referred to as the condensation coefficient, or a sticking probability. Note that the definition of mass accommodation coefficient via (2) refers only to the molecular flux entering the liquid. Evaporation, which occurs in parallel with condensation (even at growth equilibrium), results in an outgoing flux that could be described by a separate evaporation coefficient, the ratio of the actual to the maximum rate of evaporation. It is generally not possible to distinguish between the condensation and evaporation coefficients in experimental data unless the two processes can be separated unequivocally. Here, as in many previous studies of growth/evaporation kinetics (e.g., Chodes et al. 1974; Shaw and Lamb 1999), condensation and evaporation coefficients are assumed to be equal (Mozurkewich 1986; Pruppacher and Klett 1997, p. 164), as only net rates were measured. The condensation or evaporation of each volatile component is characterized by its own mass accommodation coefficient.

The thermal accommodation coefficient, α_T, accounts for the incomplete equilibration of impinging air molecules with the surface temperature (Knudsen 1911). Mathematically,

$$\alpha_T = \frac{T_{\text{out}} - T_{\text{in}}}{T_a - T_{\text{in}}}, \tag{3}$$

where T_{in} is the (kinetic energy equivalent) temperature of the gas molecules incident on the liquid surface, T_a is the liquid surface temperature, and T_{out} is the kinetic temperature of the gas molecules leaving the liquid surface. Unique values of both the thermal and the mass accommodation coefficients cannot be determined from our current evaporation experiments, so we use $\alpha_T = 0.7$, which was found in a previous study designed to yield independent measures of the two kinetic coefficients (Shaw and Lamb 1999). This value is slightly lower than the near-unity value found by Winkler et al. (2004), so sensitivity tests were performed (see section 4c).

c. Transport

The rate at which a trace gas is taken up by a liquid droplet is determined by several serial processes: gas-phase diffusion, mass accommodation at the surface, interfacial chemical equilibration, and liquid-phase diffusion [see Schwartz (1986) for details]. For systems involving more than one condensable component (e.g., H_2O and HNO_3) embedded in a noncondensable car-

rier gas, the transport of each species to or from the droplet depends to some extent on the transport of all other components in the gas phase (Heidenreich 1994; Vesala et al. 1997).

Corrections to gas-phase transport based simply on Fick's and Fourier's laws are inherently complicated (Carstens 1979). When Fick's law is applied to mass transport, for instance, one assumes that the medium is stationary and that no temperature gradients exist. Similarly, Fourier's law applies strictly to heat transport in the absence of diffusive mass transfer. However, when a droplet evaporates or grows, both concentration and temperature gradients necessarily exist. The interactions affecting mass transport include Stefan flow, thermal diffusion, and the effects of nonuniform temperature. Stefan flow, the convective (mass average) flow that affects all components, does need to be accounted for under some conditions (Hienola et al. 1999), but it is often ignored (e.g., Kulmala and Wagner 2001). For heat transport, it is the diffusion thermo effect and the energy carried with the diffusing vapor molecules that should be included. In addition to these interactions, the diffusion coefficients and thermal conductivity depend upon temperature, so they vary as a function of distance from the droplet surface under nonisothermal conditions (Rudolf et al. 2001; Nadykto et al. 2003). A rigorous calculation of the rates of heat and mass transport would account for all such effects, but many of the contributions are found to be small (Wagner 1982; Vesala et al. 1997; Mozurkewich 1986). Errors caused by the sole use of Fick's law for mass transport are negligible for growth processes under atmospheric conditions (Wagner 1982), and the transport of one component is not appreciably affected by the transport of any other component (Vesala et al. 1997).

The achievement of interfacial equilibrium is generally expected to be rapid, even for highly soluble gases (Seinfeld and Pandis 1998, p. 613). The actual vapor pressures of the volatile species at the droplet surface are therefore always close to their respective equilibrium values. Also, the liquid-phase concentrations are assumed to be uniform throughout the particle, as the time scale for internal transport is small compared with that for gas-phase transport (Rudolf et al. 2001). Overall, mass transport is limited primarily by gas-phase diffusion and mass accommodation at the surface.

The fluxes of vapors to or from a spherical particle of radius a depend on the Knudsen number $\mathrm{Kn}_i = \lambda_i/a$, where λ_i is the pressure-dependent mean free path of species i (Widmann and Davis 1997). The Knudsen number can be related to the gas-phase diffusion coefficient D_i and the average molecular speed $\bar{v}_i$ in a number of ways [see Qu and Davis (2001), and references therein], but the classical relationship,

$$\mathrm{Kn}_i = \frac{3D_i}{a\bar{v}_i}, \tag{4}$$

is commonly used (Kulmala and Wagner 2001). Small Knudsen numbers ($\mathrm{Kn} \ll 1$) correspond to the continuum regime, in which mass transport is limited by gas-phase diffusion. In this regime, the mass flux in a steady-state vapor field is based on Fick's first law, which can be written as (Pruppacher and Klett 1997, p. 504)

$$J_{c,i} = \frac{D_i m_{0,i}}{a}(n_{\infty,i} - n_{a,i}), \tag{5}$$

where $m_{0,j}$ is the mass of the molecule, $n_{\infty,i}$ is the ambient vapor number density, and $n_{a,i}$ is the equilibrium vapor number density of i immediately over the particle surface. Values of $\mathrm{Kn} \gg 1$ correspond to the kinetic regime in which mass transport is limited by surface kinetics. The mass flux of i to the particle in the kinetic regime is (Pruppacher and Klett 1997, p. 505)

$$J_{k,i} = \frac{\alpha_{M,i}\bar{v}_i m_{0,i}}{4}(n_{\infty,i} - n_{a,i}), \tag{6}$$

where $\alpha_{M,i}$ is the mass accommodation coefficient of species i. Knudsen numbers $\mathrm{Kn} \sim 1$ correspond to the transition regime, in which both gas-phase diffusion and surface kinetics are important. A full treatment of transition regime behavior needs to be based on the Boltzmann equation (Davis 1983; Seinfeld and Pandis 1998, p. 601). However, a general solution to this equation does not exist, so simplified treatments and approximations are used for the mass and heat fluxes in this regime (Davis 1983). Previous studies utilizing approximate solutions of the Boltzmann equation include those of Loyalka (1973), Sitarski and Nowakowski (1979), Qu and Davis (2001), and Qu et al. (2001). However, the models most frequently used to describe the growth of atmospheric aerosol and cloud droplets, as well as the uptake of trace gases by such particles, are semitheoretical in nature (Fuchs and Sutugin 1970) or based on flux-matching methods (Fuchs 1959; Fukuta and Walter 1970). As a general approach, the mass flux to a droplet is typically expressed as an adjustment to the continuum flux (5),

$$J_{t,i} = \frac{D_i \beta_{M,i} m_{0,i}}{a}(n_{\infty,i} - n_{a,i}), \tag{7}$$

where $\beta_{M,i}$ is a model-dependent correction factor (see Table 1 for details).

As a particle grows or evaporates, the enthalpies as-

TABLE 1. Correction factors to the continuum regime mass flux from three transition regime transport models; $\Delta_{M,i} = C\lambda_{M,i}$, with $C = 0.7$ (Pruppacher and Klett 1997, p. 506), and $\lambda_{M,i} = (3D_i/\bar{v}_i)$.

Author	Correction factor
Pruppacher and Klett (1997, p. 506)	$\beta_{m,i} = \dfrac{1}{\dfrac{a}{a+\Delta_{M,i}} + \dfrac{4D_i}{\alpha_{M,i}a\bar{v}_i}} = \dfrac{0.75\alpha_{M,i}(1+C\mathrm{Kn}_i)}{\mathrm{Kn}_i(1+C\mathrm{Kn}_i)+0.75\alpha_{M,i}}$
Fukuta and Walter (1970)	$\beta_{M,i} = \dfrac{1}{1+\dfrac{4D_i}{\alpha_{M,i}a\bar{v}_i}} = \dfrac{0.75\alpha_{M,i}}{\mathrm{Kn}_i+0.75\alpha_{M,i}}$
Fuchs and Sutugin (1970); also see Seinfeld and Pandis (1998, p. 604)	$\beta_{M,i} = \dfrac{0.75\alpha_{M,i}(1+\mathrm{Kn}_i)}{\mathrm{Kn}_i^2+\mathrm{Kn}_i+0.283\alpha_{M,i}\mathrm{Kn}_i+0.75\alpha_{M,i}}$

sociated with the phase change must be taken into account (Fukuta and Walter 1970). The droplet temperature thus always differs from the ambient temperature. For the same reasons that concentration gradients inside the droplet can be ignored, the temperature of the droplet may be taken to be uniform throughout its volume. The flux of thermal energy (heat) to or from an evolving droplet in the continuum regime is based on Fourier's law and can be expressed as (Pruppacher and Klett 1997, p. 508)

$$Q_c = \frac{k_g}{a}(T_a - T_\infty), \tag{8}$$

where k_g is the thermal conductivity of the surrounding gas, and T_∞ is the ambient temperature. In the kinetic regime, the heat flux takes the form (Pruppacher and Klett 1997, p. 509)

$$Q_k = \frac{\alpha_T n_g \bar{v}_g c_p}{4}(T_a - T_\infty), \tag{9}$$

where α_T is the thermal accommodation coefficient of carrier-gas molecules on the liquid surface, and n_g, $\bar{v}_g$, and c_p are, respectively, the number density, average molecular speed, and heat capacity at constant pressure of the surrounding gas. Fukuta and Walter (1970) replaced c_p with $c_v + k/2$, where c_v is the constant-volume heat capacity of the surrounding gas and k is the Boltzmann constant. The heat flux in the transition regime has the form

$$Q_t = \frac{k_g \beta_T}{a}(T_a - T_\infty), \tag{10}$$

where β_T is a model-dependent correction factor, analogous to $\beta_{M,i}$ in Eq. (7) (see Table 2).

d. Droplet models

Most models for atmospheric application fall into two categories: those that treat the growth of individual drops (a Lagrangian approach) and those that treat the growth of entire populations (distributions) of drops (an Eulerian approach). Many of the individual-drop studies were initiated before computer power was sufficient for detailed computations, and most of these studies simply used Langmuir's (1961) compensated diffusion coefficients for the kinetic corrections (e.g., Squires 1952; Mordy 1959). More recent studies (e.g., Clark 1973; Politovich and Cooper 1988; Kogan 1991)

TABLE 2. Correction factors to the continuum regime heat flux from three transition regime transport models.

Author	Correction factor	Definitions
Pruppacher and Klett (1997, p. 508)	$\beta_T^{(PK)} = \dfrac{1}{\dfrac{a}{a+\Delta_T} + \dfrac{4k_g}{\alpha_T a n_g \bar{v} c_p}} = \dfrac{0.75\alpha_T(1+C\mathrm{Kn})}{\mathrm{Kn}(1+C\mathrm{Kn})+0.75\alpha_T}$	$\lambda_T = \dfrac{3k_g}{n_g\bar{v}c_p}$ $\Delta_T = C\lambda_T$
Fukuta and Walter (1970)	$\beta_T^{(FW)} = \dfrac{1}{1+\dfrac{4k_g}{\alpha_T a n_g \bar{v}(c_v+0.5k)}} = \dfrac{0.75\alpha_T}{\mathrm{Kn}+0.75\alpha_T}$	$\lambda_T = \dfrac{3k_g}{n_g\bar{v}(c_v+0.5k)}$
Fuchs and Sutugin (1970); also see Rudolf et al. (2001)	$\beta_T^{(FS)} = \dfrac{0.75\alpha_T(1+\mathrm{Kn})}{\mathrm{Kn}^2+\mathrm{Kn}+0.283\alpha_T\mathrm{Kn}+0.75\alpha_T}$	$\lambda_T = \dfrac{3k_g}{n_g\bar{v}c_v}$

continued to follow this lead, despite severe criticisms by Fukuta and Walter (1970).

Whereas the methods of Squires (1952) and Mordy (1959) may still be used in some studies, most models (e.g., Roach 1976; Barkstrom 1978; Brown 1980; Paluch and Knight 1984; Cooper 1989; Austin et al. 1995) are now based on corrections derived by Fukuta and Walter (1970). Especially in Eulerian microphysical models, those that resolve the drop spectrum into fixed size bins (e.g., Feingold et al. 1994), the growth equations need to be analytically integratable, as is possible with Fukuta and Walter's (1970) kinetic corrections (Carstens 1972; Harrington et al. 2000). Less prevalently, Pruppacher and Klett's (1997) kinetic corrections are also used in numerical droplet growth models (e.g., Bott 1990; Feingold and Heymsfield 1992). Even though kinetic corrections significantly affect calculated CCN activation and the early development of drop size distributions, cloud models with assumed size spectra (i.e., gamma or lognormal distributions) tend not to use them (e.g., Ferrier 1994; Walko et al. 1995, 2000).

Three transition regime transport models seem to have been used most frequently in recent studies. The flux-matching model presented by Pruppacher and Klett (1997, 505–506) assumes that the transfer of vapor to a spherical particle is controlled by surface kinetics within the molecular boundary layer (of thickness $\Delta_M = C\lambda$ about the droplet surface) and by gas-phase diffusion at longer range. By matching the continuum regime and kinetic regime fluxes at the boundary (at radial distance $r = a + \Delta_M$), one obtains the mass flux into the droplet surface. Fukuta and Walter (1970) let the matching occur at the droplet surface (i.e., at a, implying C, $\Delta_M = 0$). Pruppacher and Klett (1997, p. 506) note that setting $C = 0.7$ lets the treatment coincide with that of Langmuir. Beyond the flux matching models, a semiempirical transition regime transport model developed by Fuchs and Sutugin (1970) has been used by many physical chemists. Fuchs and Sutugin used a semiempirical solution of the Boltzmann equation based on Sahni's (1966) transport of neutrons to a black sphere (which is analogous to complete condensation of vapor onto a spherical particle). In general, the mass flux to a droplet obtained from each of the three models discussed above is of the form given by Eq. (7), where $\beta_{M,i}$ is the model-dependent correction to the continuum regime mass flux (see Table 1). Because Fuchs and Sutugin chose to express their correction in terms of Kn, we have written the expressions for $\beta_{M,i}$ from each of the other two models in terms of the Knudsen number as well, thus facilitating a direct comparison of the correction factors.

The correction to the continuum theory, as calculated from each of the models, is shown in Fig. 1a. The approximate values of Kn corresponding to aerosol, haze, cloud, and rain particles are indicated, as is the range covered in our experiments. The correction factors from these models are overall similar. In particular, we see that the magnitude of the correction is dependent on α_M and Kn (hence on atmospheric pressure), depending on which limits of the Knudsen range one considers. For $\alpha_M > 0.1$, the mass flux does not deviate greatly from that given by the continuum theory for rain and cloud particles. However, when $\alpha_M < 0.1$, the kinetic effect can be significant, even for cloud droplets.

The relative differences between the three models considered here are shown in Fig. 1b for each of three different condensation coefficients. Significant differences show up only in the transition range, being largest when the condensation coefficient is close to unity [up to about 13% for Fukuta and Walter's (1970) model]. The cause of the difference between the models of Fukuta and Walter and of Pruppacher and Klett (1997) is the thickness ($\Delta_M = C\lambda$) of the molecular boundary layer chosen by each author. Fukuta and Walter's decision to assume the boundary layer to have negligible thickness ($C = 0$) leads to important distinctions between the various models. The use here of Pruppacher and Klett's version with $C = 0.7$ (Cunningham's constant) gives agreement with the model of Fuchs and Sutugin (1970) no worse than about 6%. Fukuta and Walter (1972), however, point out that no flux-matching model is likely to be valid when the droplet radius is less than the mean free path.

The rate of change of the mass of each volatile component in a solution droplet in a steady-state vapor field is given as

$$\frac{dm_i}{dt} = \frac{4\pi a D_i \beta_{M,i} M_i}{R}\left(\frac{p_{\infty,i}}{T_\infty} - \frac{p_{a,i}}{T_a}\right) \qquad (11)$$

(where $i = 1$ for H_2O and 2 for HNO_3). The parameters m_i, M_i, $p_{\infty,i}$, and $p_{a,j}$ are the contribution of i to the droplet mass, the molar mass of i, ambient partial pressure, and equilibrium vapor pressure over the droplet surface for component i, respectively; and R is the universal gas constant. Similarly, based on energy balance, the rate of change of the droplet temperature is

$$c_L m \frac{dT_a}{dt} = \sum_i L_i \cdot \frac{dm_i}{dt} + 4\pi a k_g \beta_T (T_\infty - T_a), \qquad (12)$$

where c_L is the specific heat of the liquid, m is the total mass of the droplet, and L_i is the enthalpy of evaporation of component i. Equations (11) and (12) form a

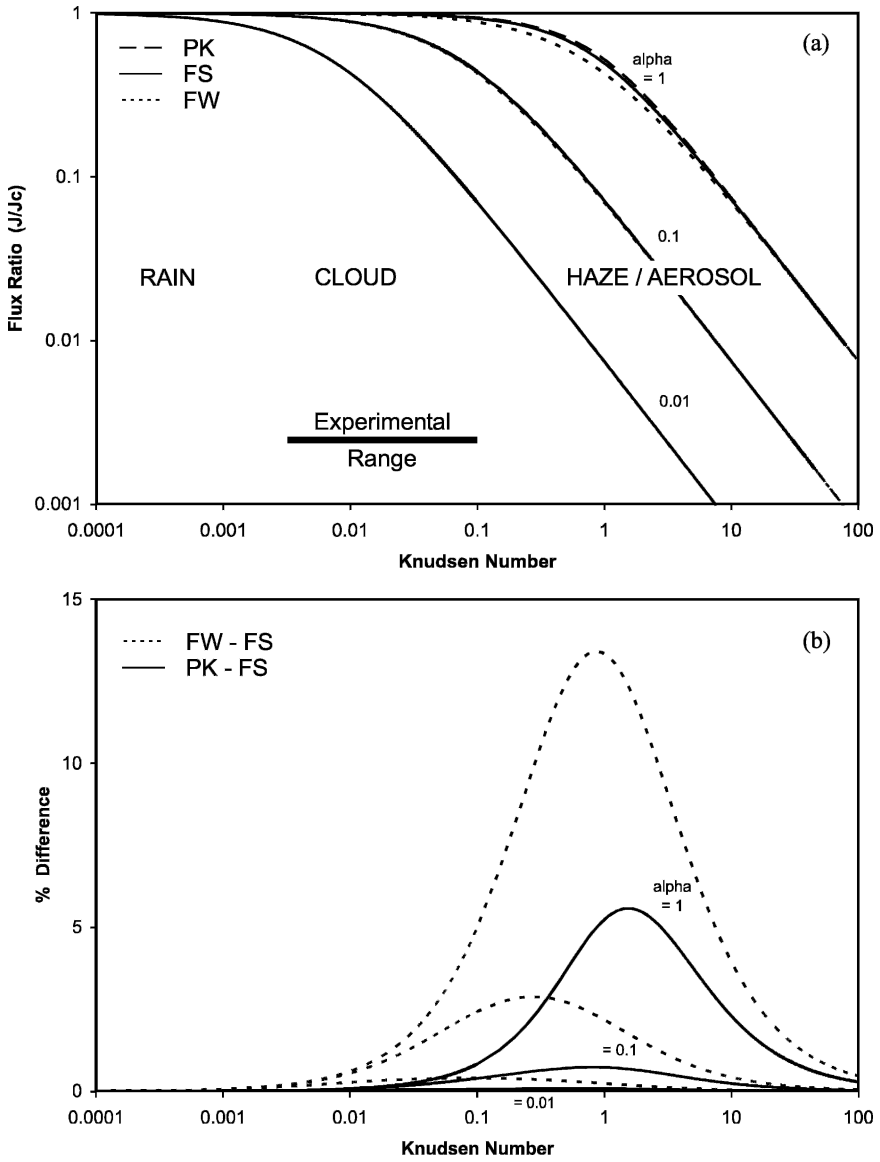

FIG. 1. (a) Correction factors to the continuum theory as calculated from the three transition regime transport models. Here, PK refers to Pruppacher and Klett (1997), FS to Fuchs and Sutugin (1970), and FW to Fukuta and Walter (1970). (b) Relative differences between the models, using Fuchs and Sutugin as reference.

closed set of equations to be solved. The equilibrium vapor pressures of H_2O and HNO_3 over the droplet surface vary with the aqueous phase composition and temperature and so must be provided by a chemical equilibrium model. In typical models (e.g., Carslaw et al. 1998), the activity coefficient of H_2O, as well as of the cations and anions in the mixture, are derived through an ion interaction approach (Carslaw et al. 1997). The chemical model of Carslaw et al. (1995) is used in the present study, which is valid over the temperature range 328 to <200 K and for acid concentrations in the range of 0 to 40 mol kg^{-1}. Droplet radius is related to the mass through the solution density (as calculated by Luo et al. 1996).

Any study focused on the kinetics of droplet growth and evaporation assumes that the droplets are out of equilibrium with their gaseous environment and thus always in the process of approaching gas–particle equilibrium. It is therefore relevant to seek the characteristic time scale for each volatile species to achieve its unique equilibrium (Meilinger et al. 1995; Meng and Seinfeld 1996; Audiffren et al. 1998). Note that such a

time scale is based on the overall mass transfer process, not simply on that for interfacial equilibrium. As shown by Meilinger et al. (1995), the time scale is inversely related to the saturation vapor pressure. The time scale for HNO_3 to achieve equilibrium in a droplet of given size is thus long compared with that for H_2O (Meilinger et al. 1995; Meng and Seinfeld 1996). This distinction proves to be important for understanding the effect of HNO_3 on droplet evaporation.

3. Methods

a. Experimental apparatus and procedures

The experiments were performed using individual charged particles localized in space within an electrodynamic balance. The principles of electrodynamic levitation have been described in the literature (see Hartung and Avedisian 1992; Allison and Kendall 1996; Davis 1997), and details of our specific system are available elsewhere (Lamb et al. 1996), so only a summary is presented here.

The cubic levitation cell, measuring 2.54 cm along each edge, is mounted inside a vacuum-jacketed environmental chamber capable of maintaining control over temperature (range −70° to about 25°C), pressure (200 hPa to atmospheric), and relative humidity (~0% to 90%). The cubic geometry offers excellent optical access and permits well-characterized, laminar gas flow around the test particle. The AC and DC voltages applied to electrodes on the six faces of the cell allow independent three-axis control over particle position near the center of the cell, where effects of chamber walls are minimal. The DC voltages could be controlled manually or via computer with a tracking board (ISCAN, Inc.) and a digital video camera (Panasonic Digital 5000) to maintain fixed particle position.

A steady laminar flow of dry gas (N_2 derived from liquid nitrogen, MG Industries), mixed with known flows of H_2O vapor, was introduced horizontally into the cell. The moisture content of the gas (≤90% relative humidity) was established by an external flow-control system, which diverted a portion of the dry nitrogen flow into a bubbler containing liquid water and a mist filter. The total flow rate was typically 5 standard $cm^3\ s^{-1}$ for experiments at atmospheric pressure and 1 standard $cm^3\ s^{-1}$ for experiments at 200 hPa, thereby maintaining a linear flow rate of slightly less than 1 $cm\ s^{-1}$ inside the cell. The absolute humidity was measured in the upstream flow with a chilled-mirror dewpoint hygrometer (±0.2°C; General Eastern Hygro-M2). The temperature of the gas entering the cell was measured close to the upstream electrode with a Type-T (copper-constantan) thermocouple referenced to a calibrated platinum-resistance thermometer (±0.02°C; Omega DP251). The gas pressure (±1 torr, Wallace and Tiernan) could be reduced to 200 hPa with a rotary-vane vacuum pump (Fisher) for investigations deeper into the transition regime.

Particles were introduced into the cell from above using a specially constructed launcher. The body of the droplet injector was constructed of 1/8" outside diameter stainless steel tubing and contained a small reservoir for the working fluid near the top. Gentle taps on a piston protruding into the reservoir forced the solution through a capillary glass tip (orifice diameter 30–50 μm) that was attached to the bottom of the launcher assembly. A moderate DC voltage (~150 V) was applied to a stainless steel cylinder surrounding the glass tip, while the top end of the injector was grounded, causing the liquid to become polarized (Lamb et al. 1996). The ejected particles thus became electrically charged, but the amount of excess charge was relatively small (~10^6 elementary units). The effect of net charge on droplet growth and evaporation was negligible. The liquid solutions were made by volumetric dilution from ultrapure reagents (HNO_3, H_2SO_4, J. T. Baker), using distilled, de-ionized water (SYBRON/Barnstead NANOpureII). Some experimental runs employed solutions derived from HPLC reagent-grade water (J. T. Baker).

An argon-ion laser (488 nm, Spectra Physics 165, ~100 mW) illuminated the levitated particle through an optical port in the bottom of the cell. Both the focused image of the particle and its structural interference pattern (Mie fringes) over a range of scattering angles from 80° to 100° were preserved simultaneously on a time-lapse video recorder (VCR, Sony) using two digital video cameras (Pulnix, Sony). A half-wave retardation plate (Edmund Scientific) was used to set the polarization of the laser beam parallel to the scattering plane and thereby enhance the contrast of the higher-order interference patterns.

Individual experimental runs began by setting the flows, temperature, and pressure inside the environmental chamber housing the levitation cell. Charged droplets were then launched into the levitation cell under conditions that were intentionally out of equilibrium with the droplet properties. Data collection started when a single droplet entered the field of view of the video cameras and became trapped in the cell. This instant was taken to be the initial time (t_0) for data analysis. The droplet was maintained in the center of the cell (by manual or computer control of the vertical DC voltage) until it evaporated beyond the electrody-

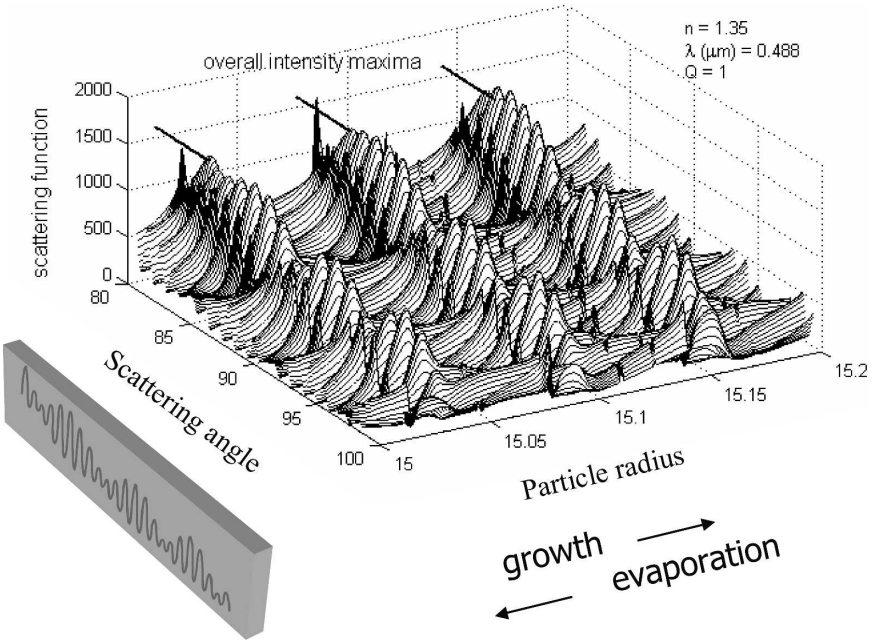

FIG. 2. Theoretical calculation of the Mie scattering function vs scattering angle and droplet radius (μm) for wavelength 488 nm, parallel polarization, and refractive index 1.35. The scattering function exhibits periodic maxima along the axis of scattering angle, as well as along the axis of the droplet radius.

namic stability point (Allison and Kendall 1996) and was no longer visible.

b. Data analysis

Droplet sizes as a function of time were determined by analysis of the recorded video data via Mie scattering theory (Bohren and Huffman 1983, chapter 4). Two methods of data analysis were used for each run, one to establish the absolute size of the droplet at one instant in time (referred to as the reference) and the other to determine how the size of the droplet evolved in time relative to this reference. The reference size was determined with an error of less than ± 0.5 μm by adjusting the size parameter in the Mie scattering calculation to produce the same number of fringes as observed in the angular range (80° to 100°) viewed by the video camera. The refractive index of the solution was derived from Luo et al. (1996).

Droplet radii away from the reference size were determined via a second optical method, one related to specific cavity resonances excited by light inside a sphere (Richardson et al. 1986). The calculated scattering intensity for representative conditions is plotted in Fig. 2 as a function of scattering angle and particle radius. Note that the scattered light intensity attains a maximum (near the line segments in Fig. 2) across all scattering angles for specific changes in droplet size. The spacing between the periodic intensity maxima is constant at 0.063 μm, thus affording a precise determination of relative size changes. The overall intensity maxima and minima manifest themselves as periodically brighter and dimmer Mie scattering patterns (flashes) in the experimental data. Therefore, if the reference radius a_{ref} is known at time t_{ref}, the radius $a(t)$ at time $t = t_{\text{ref}} + \Delta t$ can be determined to high precision (± 0.03 μm) by counting the number of overall intensity maxima n_{peaks} observed in the time interval Δt,

$$a(t) = a_{\text{ref}}(t_{\text{ref}}) + (0.063\ \mu\text{m}) n_{\text{peaks}}(\Delta t). \qquad (13)$$

The mass accommodation coefficients and other parameters were determined by fitting a model of droplet growth to the radius data. The transition-regime transport model of Pruppacher and Klett (1997, 506–509), with Cunningham's constant $C = 0.7$, was used primarily, but the models of Fukuta and Walter (1970) and Fuchs and Sutugin (1970) were also employed for comparison to ensure that the results were not sensitive to the specific model used. The equilibrium properties of the droplet at each instant were calculated from the chemical–thermodynamical model of Carslaw et al. (1995), which is based on a large body of empirical data pertaining to multicomponent solutions. The thermal accommodation coefficient (α_T) was set at 0.7 (Shaw

TABLE 3. List of transport and energy parameters used in the model calculations.

Diffusion coefficient of H_2O (Pruppacher and Klett 1997, p. 503)	$D_1 = 0.211\left(\frac{T}{T_0}\right)^{1.94}\left(\frac{p_0}{p}\right)$	D_1 in cm^2 s^{-1} T_0 = 273.15 K, T in K p_0 = 101 325.0 Pa, p in Pa
Diffusion coefficient of HNO_3 (Fuller theory; Cussler 1984, p. 112)	$D_2 = 0.1375\left(\frac{T}{T_0}\right)^{1.75}\left(\frac{p_0}{p}\right)$	D_2 in cm^2 s^{-1} T_0= 273.15 K, T in K p_0= 101 325.0 Pa, p in Pa
Thermal conductivity of moist nitrogen k_g (Pruppacher and Klett 1997, p. 508; Bird et al. 1960, p. 259)	$k_N(T) = k_{N,1} + \Gamma_N(T - T_1)$ $k_v(T) = k_{v,1} + \Gamma_v(T - T_1)$ $k_g = (1 - \gamma_1 x_v)k_N(T) + \gamma_2 x_v k_v(T)$	$k_{N,1} = 2.62 \times 10^{-2}$ J s^{-1} m^{-1} K^{-1} $\Gamma_N = 7.1 \times 10^{-5}$ J s^{-1} m^{-1} K^{-2} $k_{v,1} = 1.73 \times 10^{-2}$ J s^{-1} m^{-1} K^{-1} $\Gamma_v = 8.4 \times 10^{-5}$ J s^{-1} m^{-1} K^{-2} T_1 = 293.15 K, T in K γ_1 = 1.17, γ_2 = 1.02 Vapor mole fraction $x_v = e/p$
Water enthalpy of vaporization (Carslaw et al. 1995)	$L_1(\mu_N, T) = \sum_{j=0}^{3} A_j(T)\mu_N^j$ $A_j(T) = \sum_{i=0}^{3} B_{ij}T^i$	L_1 in kJ mol^{-1}, T in K HNO_3 molality $\mu_N \equiv \frac{\text{mol-HNO}_3}{\text{kg-H}_2\text{O}}$ B_{ij} in Table 4
Nitric acid enthalpy of vaporization (Carslaw et al. 1995)	$L_2(\mu_N, T) = \sum_{j=0}^{6} C_j(T)\mu_N^j$ $C_j(T) = \sum_{i=0}^{3} D_{ij}T^i$	L_2 in kJ mol^{-1}, T in K HNO_3 molality $\mu_N \equiv \frac{\text{mol-HNO}_3}{\text{kg-H}_2\text{O}}$ D_{ij} in Table 5

and Lamb 1999), although most droplets were reanalyzed using $\alpha_T = 1$ in order to determine the sensitivity of $\alpha(HNO_3)$ to this parameter. The formulas for the diffusion coefficients, thermal conductivity, and enthalpies of vaporization used in (11) and (12) are summarized in Tables 3, 4, and 5. In calculating the droplet energy balance, we applied the phase-change enthalpies of water and nitric acid to the fluxes of the respective vapors. The thermal conductivity of the moist gas was calculated via the formulation given by Pruppacher and Klett (1997, p. 508), but the conductivity of nitrogen was taken from Bird et al. (1960, p. 259). The specific heat of the liquid was taken to be that of water (Seinfeld and Pandis 1998, p. 778). The time-dependent mass, composition, size, and temperature of a droplet were calculated via a fourth-order Runge–Kutta scheme (Press et al. 1989, p. 550).

The selected model was initialized with a specific droplet composition and size. The initial droplet composition was first taken to be that of the bulk solution used in a particular experiment, and the initial radius was derived from the optical data. However, because neither the initial composition nor the humidity could be measured with the precision needed for data analysis, these variables were treated as free parameters (along with the mass accommodation coefficients of H_2O and HNO_3). As exemplified by Fig. 3, for each initial droplet composition, the values of $\alpha(H_2O)$, $\alpha(HNO_3)$, and dewpoint were systematically varied to give a family of curves, each yielding a local minimum. A global minimum standard deviation close to the experimental precision (± 0.03 μm) was sought between the calculated and measured droplet radii. The magnitudes of the parameters corresponding to that minimum standard deviation were taken to be the best-fit values. The uncertainty range was established by considering fitted values to be those that yielded standard deviations within a factor of 2 of the global minimum.

TABLE 4. Coefficients (B_{ij}) used to calculate the enthalpy of water vaporization at given temperature T and nitric acid molality μ_N. Based on polynomial fits of calculations from the model of Carslaw et al. (1995). See Table 3 for formulas.

i	$j = 0$	1	2	3
0	$6.4380 \times 10^{+1}$	-2.2645	1.2091×10^{-1}	-1.8770×10^{-3}
1	-1.0019×10^{-1}	1.9718×10^{-2}	-1.0311×10^{-3}	1.6485×10^{-5}
2	1.1641×10^{-4}	-5.9466×10^{-5}	3.3543×10^{-6}	-5.5032×10^{-8}
3	-3.1300×10^{-8}	6.1776×10^{-8}	-3.6027×10^{-9}	5.9730×10^{-11}

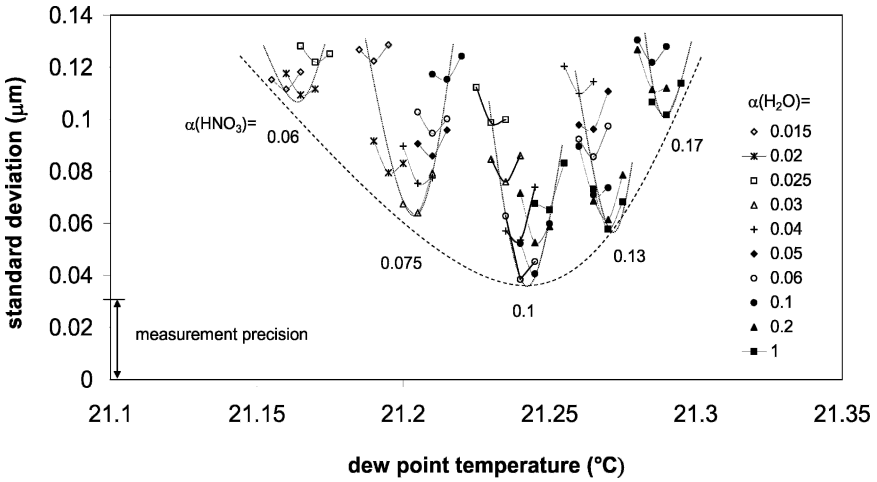

FIG. 3. Standard deviations for droplet 1.

4. Results and discussion

a. Droplet results

The environmental conditions and the analyzed droplet properties for the various experiments are tabulated in Table 6. The experiments were performed near room temperature at three different pressures (i.e., ~1 atm, ~500 hPa, and ~200 hPa), corresponding approximately to Knudsen numbers of 0.01, 0.02, and 0.05 for a 10-μm radius droplet. Data from binary solution droplets (1–26) were used to determine the mass accommodation coefficients. The inferred mass accommodation coefficients were then used in the analyses of ternary solution droplets (27 and 28). The minimum standard deviations between data and the model results for all the experiments range from 0.02 to 0.04, with an average of 0.032. More specific findings regarding the mass accommodation coefficient will be discussed later.

Figure 4 illustrates the overall evaporation behavior of the binary solutions. Droplets 1 and 2 in this series covered a wide range of initial nitric acid concentrations. The evaporation curve of a hypothetical droplet of pure water under the same conditions as droplet 1 shows the pronounced effect of HNO_3 on droplet behavior. When nitric acid is present, two stages are generally noted. The first stage is dominated by rapid adjustment toward more steady behavior. In the case of high HNO_3 concentration (droplet 2), growth first occurs until a new equilibrium with the ambient conditions is established. A weak-solution droplet (droplet 1), by contrast, evaporates monotonically, but rapidly at first. Overall evaporation is much slower in the second stage. The transition between the two stages is characterized by a kink, a sharp change in slope of the evaporation curve.

The same coupled transport-chemical thermodynamic model used for data analysis is now exploited to elucidate the underlying physics of the gas–droplet interaction. The model calculations confirm that HNO_3 and H_2O approach equilibrium on different time scales. Figure 4b shows the calculated instantaneous time scales for H_2O and HNO_3 to approach gas-particle equilibrium based on the approach of Meilinger et al. (1995). The characteristic time for H_2O (about 0.01 to 1 s) is several orders of magnitude smaller than that for HNO_3 (about 10 to 1000 s). Therefore, when an HNO_3/H_2O solution droplet is exposed to an environment that is out of equilibrium with its properties, the H_2O transfers rapidly, whereas the HNO_3 mass transfer is much slower. The two stages of evaporation are clearly seen

TABLE 5. Coefficients (D_{ij}) used to calculate the enthalpy of nitric acid vaporization at given temperature T and nitric acid molality μ_N. Based on polynomial fits of calculations from the model of Carslaw et al. (1995). See Table 3 for formulas.

i	$j = 0$	1	2	3	4	5	6
0	-6.8053×10^{1}	5.8780×10^{1}	-6.1649	3.2503×10^{-1}	-9.2921×10^{-3}	1.3775×10^{-4}	-8.2752×10^{-7}
1	1.1137	-4.9893×10^{-1}	5.0122×10^{-2}	-2.4813×10^{-3}	6.4409×10^{-5}	-8.2804×10^{-7}	4.0140×10^{-9}
2	-3.0843×10^{-3}	1.4784×10^{-3}	-1.4841×10^{-4}	7.1101×10^{-6}	-1.7233×10^{-7}	1.9435×10^{-9}	-7.0144×10^{-12}
3	3.0717×10^{-6}	-1.5231×10^{-6}	1.5284×10^{-7}	-7.2061×10^{-9}	1.6845×10^{-10}	-1.7518×10^{-12}	4.8302×10^{-15}

TABLE 6. Environmental conditions, initial droplet HNO_3 concentrations, and the mass accommodation coefficients for two different thermal accommodation coefficients.

Droplet	T (°C)	p (hPa)	T_d (°C)	wt% HNO_3	$\alpha(HNO_3)$ $\alpha_T = 0.7$	$\alpha(HNO_3)$ $\alpha_T = 1$
1	23.03	986	21.25	5.20	0.10	0.10
2[a]	23.9	986	21.34	22.5	0.05	0.05
3	27.42	986	21.11	16.2	0.08	0.08
4	27.42	986	21.14	17.0	0.11	0.11
5	27.50	986	21.27	16.6	0.12	0.12
6	27.56	986	21.39	15.8	0.15	0.15
7	27.56	986	21.17	17.0	0.10	0.10
8	27.57	986	21.19	15.8	0.11	0.11
9	27.59	986	21.07	16.6	0.12	0.12
10	27.59	986	21.14	15.8	0.14	0.15
11	26.00	477	23.36	15.0	0.13	0.13
12	26.04	482	23.62	15.0	0.21	0.20
13	26.04	482	23.52	15.4	0.25	0.25
14	27.36	481	23.85	7.80	0.15	0.15
15	27.38	485	23.89	7.00	0.13	0.13
16	27.06	225	22.69	15.8	0.20	0.20
17	25.01	209	20.73	10.1	0.46	0.45
18	22.35	207	19.65	10.1	0.29	0.30
19	22.35	207	19.62	10.1	0.28	0.29
20	22.35	207	19.59	10.1	0.35	0.35
21	22.37	209	19.53	10.1	0.32	0.33
22	22.37	209	19.51	10.1	0.35	0.35
23	22.37	209	19.47	10.1	0.40	0.40
24	22.47	213	19.50	10.1	0.27	0.27
25	22.47	213	19.58	10.1	0.45	0.45
26	22.47	213	19.36	10.1	0.23	0.23
27[b]	23.67	986	21.65	3.50	0.11	
28[c]	22.73	986	18.93	0	0.11	

[a] Temperature measurement with limited precision of ±0.2°C.
[b] Droplet also contained 6.23% of H_2SO_4 initially.
[c] Droplet also contained 6.50% H_2SO_4 initially and exposed to 3.5 ppm gas-phase HNO_3.

in the calculated ratio of water-to-nitric acid fluxes, $(dm_1/dt)/(dm_2/dt)$ (Fig. 4c). The concentration of H_2O in the droplet changes rapidly in the first stage, as shown in Fig. 4d. The rapid change in liquid-phase HNO_3 concentration in this early stage is caused mainly by the change of droplet volume from H_2O mass transfer, rather than by the mass transfer of HNO_3 itself. The second stage of evaporation starts when the H_2O-to-HNO_3 mass flux ratio is constant (Fig. 4c), resulting in constant concentration until the droplet totally evaporates (Fig. 4d). Evaporation of nitric acid solution droplets thus proceeds azeotropically during most of their lifetimes (Atkins 1986, p. 181). H_2O tends to remain in quasi-equilibrium with the environmental conditions as HNO_3 slowly volatilizes throughout the second stage.

Ternary $H_2SO_4/HNO_3/H_2O$ droplets exhibit similar evaporation characteristics, except that a residual droplet always remains due to the nonvolatile nature of sulfate. As shown for droplet 27 in Figs. 5a,b, H_2O responds rapidly to the out-of-equilibrium conditions during the first stage. This rapid loss of water relative to that of nitric acid (Fig. 5c) causes the solution to con-

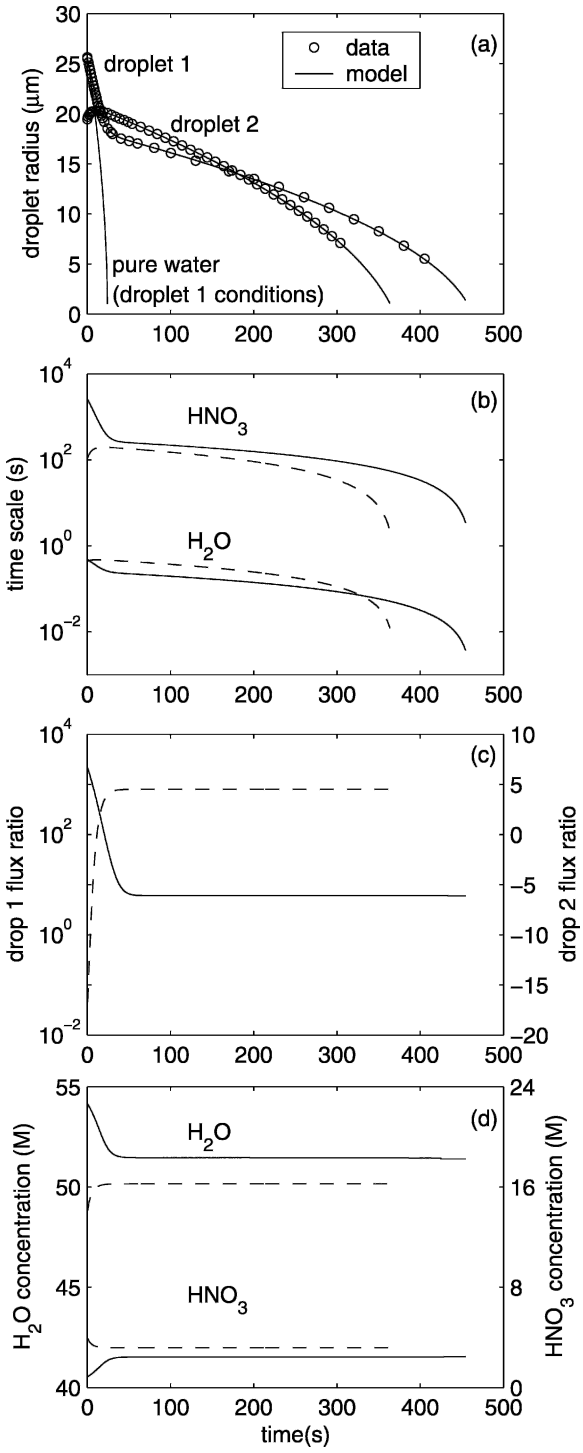

FIG. 4. (a)–(d) Evaporation/growth behavior of binary solution droplets. To distinguish the analyses of droplets 1 and 2, solid lines in (b)–(d) represent droplet 1, while the dashed lines represent droplet 2.

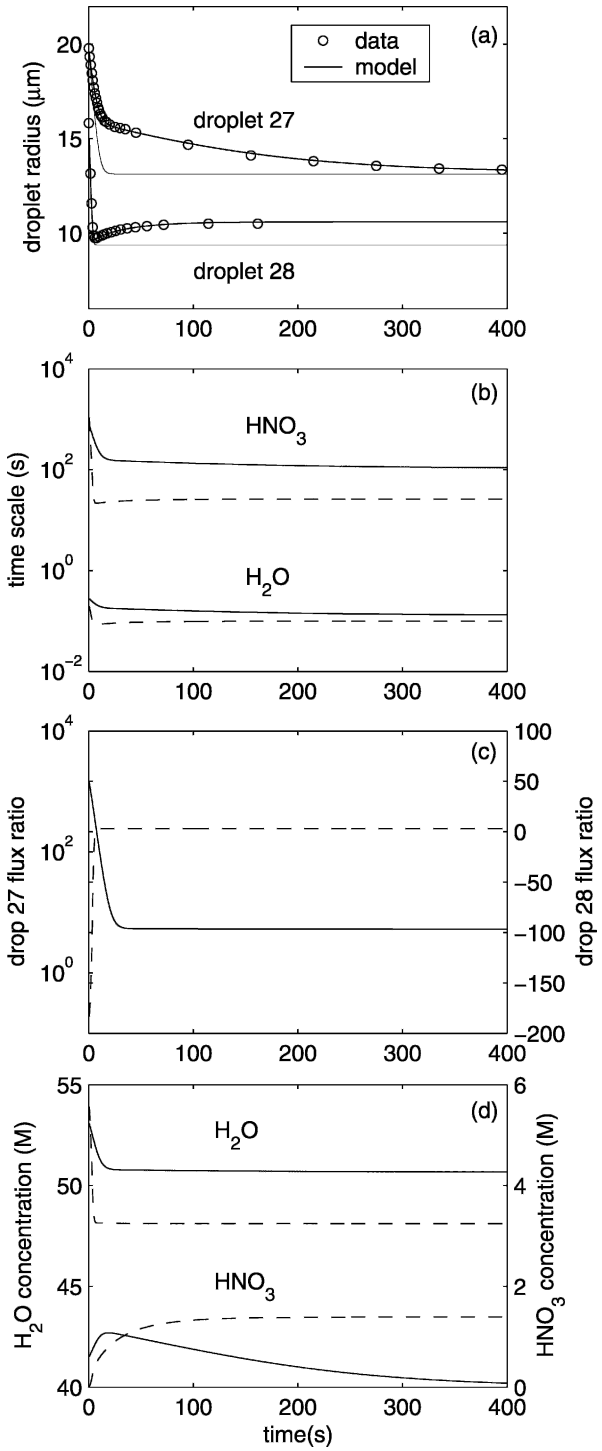

FIG. 5. Evaporation/growth behavior of ternary solution droplets. (a) The thin curves represent sulfate particles without HNO_3 present. (b)–(d) Solid lines represent droplet 27, while the dashed lines represent droplet 28.

centrate initially (Fig. 5d), but then the HNO_3 concentration slowly decreases as it volatilizes into an environment devoid of HNO_3 vapor. The concentration of water, however, remains constant as the one acid replaces the other. Droplet 28, by contrast, initially contained no nitric acid, instead being exposed only to gas-phase HNO_3. Beyond an initial loss of water, droplet 28 actually gained mass in the second stage as it absorbed HNO_3 from the gas phase. The effect of HNO_3 on the behavior of sulfate particles is indicated by comparing the data with the thin curves in Fig. 5a, which pertain to behavior were no nitric acid to have been present.

b. Alternative transport models

The excellent agreement between the model calculations and the data from the four droplets shown in Figs. 4 and 5 validates the overall structure of the coupled modeling system. Four widely varying scenarios were generated, and in each case the model captured all of the features of droplet evaporation, always using a consistent set of model parameters. Agreement was strong even in the case of droplet 2, which exhibited a period of transient growth as water was taken up while the nitric acid concentration was high and reduced the water activity greatly. Simply changing the initial and environmental conditions to the appropriate values was sufficient to generate agreement. One may argue about the specific values chosen for the model parameters, but the overall form of the equations used to calculate droplet behavior is sound.

Given that most of the analyses have been based on the model of Pruppacher and Klett (1997), it is natural to ask whether predicted droplet behavior or the inferred magnitudes of $\alpha(HNO_3)$ would be changed had alternative transition regime transport models been used. The transport models of Pruppacher and Klett (1997), Fukuta and Walter (1970), and Fuchs and Sutugin (1970) were compared directly and also used for some of the data analysis. As shown in Fig. 1, each of the three models exhibits similar behavior over wide ranges of Knudsen number. Only in the transition regime (near Kn $\sim$1) and for large mass accommodation coefficients do modest differences appear. Fukuta and Walter (1972) make the point that flux-matching models may be invalid at large Kn, but their model nevertheless agrees well with the Fuchs and Sutugin model, which is based on a more complete treatment of vapor transport (Chang and Davis 1976; Vesala et al. 2001). The underlying chemical thermodynamic model is implicitly validated too, although our analysis procedure would compensate for minor biases in calculated activities.

Data analysis using different transition regime transport models does not significantly affect the determination of $\alpha(HNO_3)$. However, because the continuum regime theory should account for higher-order phenomena (Wagner 1982), whereas the models used here are based only on Fick's and Fourier's laws, continued study is warranted.

c. The accommodation coefficients

The values of $\alpha(HNO_3)$ determined from the 26 binary solution experiments in this study are summarized in Fig. 6. The average magnitudes of $\alpha(HNO_3)$ exhibit an apparent dependence on total pressure: 0.11 ± 0.03 at atmospheric pressure, 0.17 ± 0.05 at 500 hPa, and 0.33 ± 0.08 at 200 hPa. We expect no direct pressure dependence to the mass-accommodation process, so other parameters may have varied with pressure and possibly influenced mass accommodation. For example, the diffusion coefficients are explicitly dependent on pressure, as is the thermal diffusivity, nonlinear variations that could affect the droplet composition and hence the accommodation coefficient. Also, the saturation ratio over the droplet surface changes with ambient pressure and possibly alters the efficiency of molecular exchange across the interface (Lamb et al. 2004). This matter will be explored in greater detail in the future.

The techniques used in this study, unlike the approach taken by Winkler et al. (2004), cannot independently determine the thermal accommodation coefficient (α_T). The value used here (0.7) is based on prior experiments that did allow independent determination of mass and thermal accommodation coefficients (Shaw and Lamb 1999). Nevertheless, other experiments yield values near unity (Winkler et al. 2004), so we have rerun the analyses using $\alpha_T = 1$ in order to provide a measure of the sensitivity of $\alpha(HNO_3)$ to this parameter (see Table 6). Note that the analyzed values of $\alpha(HNO_3)$ are very insensitive to the choice of α_T over this range.

Overall, the magnitudes of $\alpha(HNO_3)$ determined here are consistent with those derived from completely different methods (Van Doren et al. 1990; Ponche et al. 1993). Our $\alpha(HNO_3)$ values are slightly lower than those of Rudolf et al. (2001), who put 0.3 as the lower limit based on binary condensation to small particles in an expansion chamber. But, the same arguments we have tentatively used to explain the empirical pressure dependence also lead us to expect $\alpha(HNO_3)$ to be relatively large over small particles at high supersaturations (Lamb et al. 2004).

The values of the water accommodation coefficient arising in this study vary widely and are not useful in themselves. Specific values of $\alpha(H_2O)$ are needed for data analysis, but large variations (within the range 0.01 to 1) work equally well, mainly because $\alpha(H_2O)$ has little impact on the overall evaporation process when nitric acid is present. Water evaporation limits droplet evaporation only early in the process, when the droplet size is still large compared with the molecular mean free path in the gas phase. By the time a droplet becomes small toward the end of each run, the evaporation is limited by the relatively high concentration of HNO_3. The value of $\alpha(H_2O)$ is moreover convoluted with the analyzed moisture content of the ambient gas, so any change in $\alpha(H_2O)$ is compensated for by a slightly different analyzed dewpoint temperature. The net result is virtually no impact of $\alpha(H_2O)$ on the analyzed $\alpha(HNO_3)$ and no opportunities to compare our findings with those from experiments employing pure water (e.g., Li et al. 2001; Winkler et al. 2004). Future work will be focused on the mass accommodation of pure water.

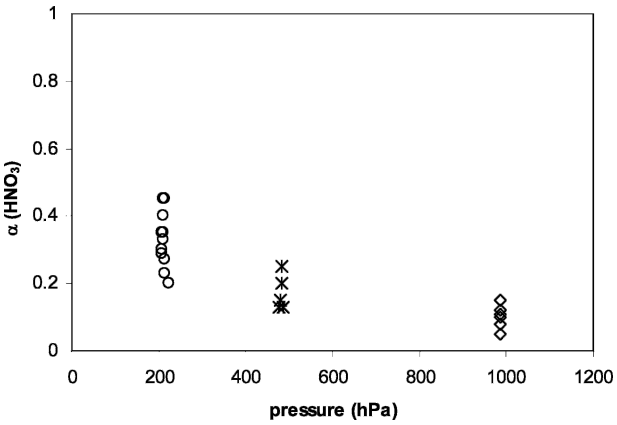

FIG. 6. Summary of $\alpha(HNO_3)$ from the 26 binary solution experiments at different pressures.

5. Summary and conclusions

This study presents new experimental data appropriate for verifying models used to simulate the growth and evaporation of droplets under atmospheric conditions. The mass accommodation coefficients of HNO_3 on droplets of various binary (HNO_3/H_2O) and ternary ($H_2SO_4/HNO_3/H_2O$) solutions have been determined by fitting precise sets of evaporation data taken at room temperature and various pressures. The analysis procedure requires the environmental temperature and dewpoint to be determined to high precision (± 0.01 K). The magnitude of the nitric acid mass accommodation coefficient was found to vary with pressure: ~ 0.11 at atmospheric pressure, ~ 0.17 at 500 hPa and ~ 0.33 at

200 hPa, suggesting that the mass accommodation process might vary with the environmental conditions. Further research is needed to resolve the molecular mechanism of mass accommodation.

Both the data and the model calculations show that the coevaporation of two volatile components (HNO_3/H_2O) occurs in two stages. These findings confirm that each volatile species has a unique time scale for approaching gas–droplet equilibrium and validate the coupling of a chemical thermodynamic model to a transition regime kinetics model for atmospheric applications. Despite ongoing criticism, the flux-matching model of Pruppacher and Klett (1997, p. 506) was able to provide robust agreement with the experimental data. The models of Fukuta and Walter (1970) and Fuchs and Sutugin (1970) yielded comparable mass accommodation coefficients within experimental error. The coupled modeling system is also rich in auxiliary information useful for diagnosing chemical and physical cloud processes.

Acknowledgments. This research was supported by the National Science Foundation under Grants ATM-9981511 and ATM-0234211. We are grateful to Simon Clegg for providing the code for the chemical thermodynamic model and to Ulrich Krieger for sharing the code for solution densities and refractive indices. We also thank Raymond Shaw for helpful discussions, and Paul Smidansky for assistance with data analysis. Helpful suggestions from the anonymous reviewers are also appreciated.

REFERENCES

Allison, E. E., and B. R. F. Kendall, 1996: Cubic electrodynamic levitation trap with transparent electrodes. *Rev. Sci. Instrum.,* **67,** 3806–3812.

Atkins, P. W., 1986: *Physical Chemistry*. W.H. Freeman and Company, 857 pp.

Audiffren, N., M. Renard, E. Buisson, and N. Chaumerliac, 1998: Deviations from the Henry's law equilibrium during cloud events: A numerical approach of the mass transfer between phases and its specific numerical effects. *Atmos. Res.,* **49,** 139–161.

Austin, P. H., S. Siems, and Y. Wang, 1995: Constraints on droplet growth in radiatively cooled stratocumulus. *J. Geophys. Res.,* **100,** 14 231–14 242.

Barkstrom, B. R., 1978: Some effects of 8–10 mm radiant energy transfer on the mass and heat budgets of cloud droplets. *J. Atmos. Sci.,* **35,** 665–673.

Bird, R. B., W. E. Stewart, and E. N. Lightfoot, 1960: *Transport Phenomena*. John Wiley and Sons, 780 pp.

Bohren, C. F., and D. R. Huffman, 1983: *Absorption and Scattering of Light by Small Particles*. John Wiley and Sons, 530 pp.

Bott, A., 1990: On the influence of the physico-chemical properties of aerosols on the life cycle of radiation fogs. *J. Aerosol Sci.,* **21,** S279–S282.

Brown, R., 1980: A numerical study of radiation fog with an explicit formulation of the microphysics. *Quart. J. Roy. Meteor. Soc.,* **106,** 781–802.

Carslaw, K. S., B. P. Luo, S. L. Clegg, Th. Peter, P. Brimblecombe, and P. J. Crutzen, 1994: Stratospheric aerosol growth and HNO_3 gas phase depletion from coupled HNO_3 and water uptake by liquid particles. *Geophys. Res. Lett.,* **21,** 2479–2482.

——, S. L. Clegg, and P. Brimblecombe, 1995: A thermodynamic model of the system HCl - HNO_3 - H_2SO_4 - H_2O, including solubilities of HBr, from <200 to 328 K. *J. Phys. Chem.,* **99,** 11 557–11 574.

——, Th. Peter, and S. L. Clegg, 1997: Modeling the composition of liquid stratospheric aerosols. *Rev. Geophys.,* **35,** 125–154.

——, and Coauthors, 1998: Particle microphysics and chemistry in remotely observed mountain polar stratospheric clouds. *J. Geophys. Res.,* **103,** 5785–5796.

Carstens, J. C., 1972: Comments on "Kinetics of hydrometeor growth from a vapor-spherical model." *J. Atmos. Sci.,* **29,** 588–591.

——, 1979: Drop growth in the atmosphere by condensation: Application to cloud physics. *Adv. Colloid Interface Sci.,* **10,** 285–314.

Chang, R., and E. J. Davis, 1976: Knudsen aerosol evaporation. *J. Colloid Interface Sci.,* **54,** 352–363.

Charlson, R. J., J. H. Seinfeld, A. Nenes, M. Kulmala, A. Laaksonen, and M. C. Fachini, 2001: Reshaping the theory of cloud formation. *Science,* **292,** 2025–2026.

Chodes, N., J. Warner, and A. Gagin, 1974: A determination of the condensation coefficient of water from the growth rate of small cloud droplets. *J. Atmos. Sci.,* **31,** 1351–1357.

Clark, T. L., 1973: Numerical modeling of the dynamics and microphysics of warm cumulus convection. *J. Atmos. Sci.,* **30,** 857–878.

Clegg, S. L., and P. Brimblecombe, 1990: Equilibrium partial pressure and mean activity and osmotic coefficients of 0-100% nitric acid as a function of temperature. *J. Phys. Chem.,* **94,** 5369–5380.

——, P. Brimblecombe, and A. S. Wexler, 1998: Thermodynamic model of the system H^+-NH_4^+-SO_4^{2-}-NO_3^--H_2O at tropospheric temperatures. *J. Phys. Chem. A,* **102,** 2137–2154.

Cooper, W. A., 1989: Effects of variable droplet growth histories on droplet size distributions. Part I: Theory. *J. Atmos. Sci.,* **46,** 1301–1311.

Cussler, E. L., 1984: *Diffusion, Mass Transfer in Fluid Systems*. Cambridge University Press, 525 pp.

Davidovits, P., J. T. Jayne, S. X. Duan, D. R. Worsnop, M. S. Zahniser, and C. E. Kolb, 1991: Uptake of gas molecules by liquids: A model. *J. Phys. Chem.,* **95,** 6337–6340.

——, J. H. Hu, D. R. Worsnop, M. S. Zahniser, and C. E. Kolb, 1995: Entry of gas molecules into liquids. *Faraday Discuss.,* **100,** 65–82.

Davis, E. J., 1983: Transport phenomena with single aerosol particles. *Aerosol Sci. Technol.,* **2,** 121–144.

——, 1997: A history of single aerosol particle levitation. *Aerosol Sci. Technol.,* **26,** 212–254.

Feingold, G., and A. J. Heymsfield, 1992: Parameterizations of condensational growth of droplets for use in general circulation models. *J. Atmos. Sci.,* **49,** 2325–2342.

——, and S. M. Kreidenweis, 2002: Cloud processing of aerosol as modeled by a large eddy simulation with coupled microphysics and aqueous chemistry. *J. Geophys. Res.,* **107,** 4687, doi:10.1029/2002JD002054.

——, B. Stevens, W. R. Cotton, and R. L. Walko, 1994: An ex-

plicit cloud microphysics/LES model designed to simulate the Twomey effect. *Atmos. Res.,* **33,** 207–233.

Ferrier, B. S., 1994: A double moment multiple phase four class bulk ice scheme. Part I: Description. *J. Atmos. Sci.,* **51,** 249–280.

Fuchs, N. A., 1959: *Evaporation and Droplet Growth in Gaseous Media*. Pergamon, 72 pp.

——, and A. G. Sutugin, 1970: *Highly Dispersed Aerosols*. Ann Arbor Science Publishers, 105 pp.

Fukuta, N., and L. A. Walter, 1970: Kinetics of hydrometeor growth from a vapor–spherical model. *J. Atmos. Sci.,* **27,** 1160–1172.

——, and ——, 1972: Reply. *J. Atmos. Sci.,* **29,** 591–592.

Harrington, J. Y., G. Feingold, and W. R. Cotton, 2000: Radiative impacts on the growth of a population of drops within simulated summertime arctic stratus. *J. Atmos. Sci.,* **57,** 766–785.

Hartung, W. H., and C. T. Avedisian, 1992: On the electrodynamic balance. *Proc. Roy. Soc. London,* **A437,** 237–266.

Hegg, D. A., 2000: Impact of gas-phase HNO_3 and NH_3 on microphysical processes in atmospheric clouds. *Geophys. Res. Lett.,* **27,** 2201–2204.

Heidenreich, S., 1994: Condensational droplet growth in the continuum regime—A critical review for the system air-water. *J. Aerosol Sci.,* **25,** 49–59.

Hienola, J., M. Kulmala, and A. Laaksonen, 1999: Influence of nitric acid vapor on cloud particle formation at low temperatures in troposphere. *J. Aerosol Sci.,* **30,** S23–S24.

Houghton, J. T., Y. Ding, D. J. Griggs, M. Noguer, P. J. van der Linden, and D. Xiaosu, Eds., 2001: *Climate Change 2001: The Scientific Basis.* Cambridge University Press, 785 pp.

Jaecker-Voirol, A., J. L. Ponche, and P. Mirabel, 1990: Vapor pressures in the ternary system water-nitric acid-sulfuric acid at low temperatures. *J. Geophys. Res.,* **95,** 11 857–11 863.

Kim, Y. P., J. H. Seinfeld, and P. Saxena, 1993: Atmospheric gas-aerosol equilibrium. I. Thermodynamic model. *Aerosol Sci. Technol.,* **19,** 157–181.

Knudsen, M., 1911: Molecular heat conductivity of gases and the coefficient of accommodation. *Ann. Phys.,* **34,** 593–656.

Kogan, Y. L., 1991: The simulation of a convective cloud in a 3-D model with explicit microphysics. Part I: Model description and sensitivity experiments. *J. Atmos. Sci.,* **48,** 1160–1189.

Kolb, C. E., P. Davidovits, J. T. Jayne, Q. Shi, and D. R. Worsnop, 2002: Kinetics of trace gas uptake by liquid surfaces. *Prog. React. Kin. Mech.,* **27,** 1–46.

Korhonen, P., M. Kulmala, and T. Vesala, 1996: Model simulation of the amount of soluble mass during cloud droplet formation. *Atmos. Environ.,* **30,** 1773–1785.

Kulmala, M., and P. E. Wagner, 2001: Mass accommodation and uptake coefficients—A quantitative comparison. *J. Aerosol Sci.,* **32,** 833–841.

——, A. Laaksonen, P. Korhonen, T. Vesala, T. Ahonen, and J. C. Barrett, 1993: The effect of atmospheric nitric acid vapor on cloud condensation nucleus activation. *J. Geophys. Res.,* **98,** 22 949–22 958.

——, P. Korhonen, A. Laaksonen, and T. Vesala, 1995: Changes in cloud properties due to NO_x emissions. *Geophys. Res. Lett.,* **22,** 239–242.

——, A. Laaksonen, R. J. Charlson, and P. Korhonen, 1997: Clouds without supersaturation. *Nature,* **388,** 336–337.

Laaksonen, A., P. Korhonen, M. Kulmala, and R. J. Charlson, 1998: Modification of the Köhler equation to include soluble trace gases and slightly soluble substances. *J. Atmos. Sci.,* **55,** 853–862.

Lamb, D., A. M. Moyle, and W. H. Brune, 1996: The environmental control of individual aqueous particles in a cubic electrodynamic levitation system. *Aerosol Sci. Technol.,* **24,** 263–278.

——, ——, and H. Xue, 2004: Droplet evaporation: Theoretical implications of recent data for binary nitric acid solutions. Preprints, *14th Int. Conf. on Clouds and Precipitation*, Bologna, Italy, ICCP, 462–464.

Langmuir, I., 1961: *The Collected Works of Irving Langmuir*. 12 vols. Oxford University Press.

Li, Y.-M., and J. Coull, 1948: The prediction of vapour-liquid equilibria for ternary mixtures from the data of binary systems. *J. Inst. Petrol.,* **34,** 692–704.

Li, Y. Q., P. Davidovits, Q. Shi, J. T. Jayne, C. E. Kolb, and D. R. Worsnop, 2001: Mass and thermal accommodation coefficients of $H_2O(g)$ on liquid water as a function of temperature. *J. Phys. Chem.,* **105A,** 10 627–10 634.

Loyalka, S. K., 1973: Condensation on a spherical droplet. *J. Chem. Phys.,* **58,** 354–356.

Luo, B., U. K. Krieger, and Th. Peter, 1996: Densities and refractive indices of $H_2SO_4/HNO_3/H_2O$ solutions to stratospheric temperatures. *Geophys. Res. Lett.,* **23,** 3707–3710.

Meilinger, S. K., T. Koop, B. P. Luo, T. Huthwelker, K. S. Carslaw, U. Krieger, P. J. Crutzen, and Th. Peter, 1995: Size-dependent stratospheric droplet composition in lee wave temperature fluctuations and their potential role in PSC freezing. *Geophys. Res. Lett.,* **22,** 3031–3034.

Meng, Z., and J. H. Seinfeld, 1996: Time scales to achieve atmospheric gas-aerosol equilibrium for volatile species. *Atmos. Environ.,* **30,** 2889–2900.

Mordy, W., 1959: Computations of the growth by condensation of a population of cloud droplets. *Tellus,* **11,** 16–44.

Mozurkewich, M., 1986: Aerosol growth and the condensation coefficient for water: A review. *Aerosol Sci. Technol.,* **5,** 223–236.

Nadykto, A. B., E. R. Shchukin, M. Kulmala, K. E. J. Lehtinen, and A. Laaksonen, 2003: Evaporation and condensational growth of liquid droplets in nonisothermal gas mixtures. *Aerosol Sci. Technol.,* **37,** 315–324.

Nenes, A., R. J. Charlson, M. C. Facchini, M. Kulmala, A. Laaksonen, and J. H. Seinfeld, 2002: Can chemical effects on cloud droplet number rival the first indirect effect? *Geophys. Res. Lett.,* **29,** 1848, doi:10.1029/2002GL015295.

Paluch, I. R., and C. A. Knight, 1984: Mixing and the evolution of cloud droplet size spectra in a vigorous continental cumulus. *J. Atmos. Sci.,* **41,** 1801–1815.

Politovich, M. K., and W. A. Cooper, 1988: Variability of the supersaturation in cumulus clouds. *J. Atmos. Sci.,* **45,** 1651–1664.

Ponche, J. L., C. George, and P. Mirabel, 1993: Mass transfer at the air/water interface: Mass accommodation coefficients of SO_2, HNO_3, NO_2, and NH_3. *J. Atmos. Chem.,* **16,** 1–21.

Press, W. H., B. P. Flannery, S. A. Teukolsky, and W. T. Vetterling, 1989: *Numerical Recipes (FORTRAN Version)*. Cambridge University Press, 702 pp.

Pruppacher, H. R., and J. D. Klett, 1997: *Microphysics of Clouds and Precipitation*. Kluwer Academic, 954 pp.

Qu, X., and E. J. Davis, 2001: Droplet evaporation and condensation in the near-continuum regime. *J. Aerosol Sci.,* **32,** 861–875.

——, ——, and B. D. Swanson, 2001: Non-isothermal droplet evaporation and condensation in the near-continuum regime. *J. Aerosol Sci.,* **32,** 1315–1339.

Richardson, C. B., R. L. Hightower, and A. L. Pigg, 1986: Optical

measurement of the evaporation of sulfuric acid droplets. *Appl. Opt.,* **25,** 1226–1229.

Roach, W. T., 1976: On the effect of radiative exchange on the growth by condensation of a cloud or fog droplet. *Quart. J. Roy. Meteor. Soc.,* **102,** 361–372.

Rogers, R. R., and M. K. Yau, 1989: *A Short Course in Cloud Physics*. Pergamon Press, 293 pp.

Rosenfeld, D., 2000: Suppression of rain and snow by urban and industrial air pollution. *Science,* **287,** 1793–1796.

Rudolf, R., A. Vrtala, M. Kulmala, T. Vesala, Y. Viisanen, and P. E. Wagner, 2001: Experimental study of sticking probabilities for condensation of nitric acid-water vapor mixtures. *J. Aerosol Sci.,* **32,** 913–932.

Sahni, D. C., 1966: The effect of a black sphere on the flux distribution of an infinite moderator. *J. Nucl. Energy,* **20,** 915–920.

Schwartz, S. E., 1986: Mass-transport considerations pertinent to aqueous phase reactions of gases in liquid-water clouds. *Chemistry of Multiphase Atmospheric Systems,* NATO ASI Series, 415–471.

Seinfeld, J. H., and S. N. Pandis, 1998: *Atmospheric Chemistry and Physics*. John Wiley and Sons, 1326 pp.

Shaw, R. A., and D. Lamb, 1999: Experimental determination of the thermal accommodation and condensation coefficients of water. *J. Chem. Phys.,* **111,** 10 659–10 663.

Sitarski, M., and B. Nowakowski, 1979: Condensation rate of trace vapor on Knudsen aerosols from the solution of the Boltzmann equation. *J. Colloid Interface Sci.,* **72,** 113–122.

Squires, P., 1952: The growth of cloud drops by condensation. 1. General characteristics. *Austr. J. Sci. Res. Ser. A,* **5,** 59–86.

Stumm, W., and J. J. Morgan, 1981: *Aquatic Chemistry*. John Wiley, 780 pp.

Tabazadeh, A., R. P. Turco, K. Drdla, and M. Z. Jacobson, 1994: A study of Type I polar stratospheric cloud formation. *Geophys. Res. Lett.,* **21,** 1619–1622.

Tang, I. N., 1980: On the equilibrium partial pressures of nitric acid and ammonia in the atmosphere. *Atmos. Environ.,* **14,** 819–828.

Van Doren, J. M., L. R. Watson, P. Davidovits, D. R. Worsop, M. S. Zahniser, and C. E. Kolb, 1990: Temperature dependence of the uptake coefficients of HNO_3, HCl, and N_2O_5 by water droplets. *J. Phys. Chem.,* **94,** 3265–3269.

Vesala, T., M. Kulmala, R. Rudolf, A. Vrtala, and P. E. Wagner, 1997: Models for condensational growth of binary aerosol particles. *J. Aerosol Sci.,* **28,** 565–598.

——, A. U. Hannemann, B. P. Luo, M. Kulmala, and T. Peter, 2001: Rigorous treatment of time-dependent trace gas uptake by droplets including bulk diffusion and surface accommodation. *J. Aerosol Sci.,* **32,** 843–860.

Walko, R. L., W. R. Cotton, J. L. Harrington, and M. P. Meyers, 1995: New RAMS cloud microphysics parameterization. Part I: The single-moment scheme. *Atmos. Res.,* **38,** 29–62.

——, ——, G. Feingold, and B. Stevens, 2000: Efficient computation of vapor and heat diffusion between hydrometeors in a numerical model. *Atmos. Res.,* **53,** 171–183.

Wagner, P. E., 1973: Optical determination of the size of fast-growing water droplets in an expansion cloud chamber. *J. Colloid Interface Sci.,* **44,** 181–183.

——, 1982: Aerosol growth by condensation. *Aerosol Physics II, Chemical Physics of Microparticles*, W. H. Marlow, Ed., Springer-Verlag, 129–178.

Widmann, J. F., and E. J. Davis, 1997: Mathematical models of the uptake of ClONO2 and other gases by atmospheric aerosols. *J. Aerosol Sci.,* **28,** 87–106.

Winkler, P. M., A. Vrtala, P. E. Wagner, M. Kulmala, K. E. J. Lehtinen, and T. Vesala, 2004: Mass and thermal accommodation during gas-liquid condensation of water. *Phys. Rev. Lett.,* **93,** 075701-1–075701-4.

Xue, H., and G. Feingold, 2004: A modeling study of the effect of nitric acid on cloud properties. *J. Geophys. Res.,* **109,** D18204, doi:10.1029/2004JD004750.

Zhang, R., P. J. Wooldridge, and M. J. Molina, 1993: Vapor pressure measurements for the $H_2SO_4/HNO_3/H_2O$ and $H_2SO_4/HCl/H_2O$ systems: Incorporation of stratospheric acids into background sulfate aerosols. *J. Phys. Chem.,* **97,** 8541–8548.